



Article submitted to journal

Subject Areas:

heritage structure, extreme waves,
lighthouse

Keywords:

extreme wave, wave breaking, wave
loading

Author for correspondence:

e-mail:

jean.francois.filipot@ite-fem.org

La Jument Lighthouse: a real scale laboratory for the study of giant waves and of their loading on marine structures

J.-F. Filipot¹, P. Guimaraes², F. Leckler², J. Hortsmann³, R. Carrasco³, E. Leroy⁴, N. Fady⁴, M. Prevosto⁵, V. Roeber⁶, A. Benetazzo⁷, C. Raoult², M. Franzetti⁸, A. Varing¹, N. Le Dantec⁴

¹France Energies Marines, Plouzané, France, ²Shom, Brest, France, ³HZG, Geestacht, Germany, ⁴Cerema, Plouzané, France, ⁵Ifremer, Plouzané, France ⁷CNR, Venice, Italy, ⁸IUEM-LGO, Plouzané, France

This paper presents observations from an experiment designed to progress in the understanding of the relation between extreme breaking waves and their mechanical loading on heritage lighthouses at sea. The experiment, conducted from La Jument, an iconic French lighthouse at sea, featured several records of wave, current, bathymetry and structure accelerations acquired during severe storm conditions, with individual waves as high as 23.6m. The data analysis of the observations focuses on a storm event marked by a strong peak in the horizontal accelerations measured inside La Jument. Thanks to stereo-video wave measurements synchronized to the acceleration record we were able to identify and describe the breaking wave responsible for this intense loading. Our observations suggest that this giant wave (19 m high) is the only one with a crest elevation high enough to pass over the substructure and hit directly the lighthouse tower. This paper reveals the potential for conducting ambitious field experiments from lighthouses at sea so as to fill the lack of storm waves and wave loading observations. This offers a possible second service life for these heritage structures as *in situ* laboratories dedicated to the study of the coastal hydrodynamics and its interactions with marine structures.

© The Authors. Published by the Royal Society under the terms of the Creative Commons Attribution License <http://creativecommons.org/licenses/by/4.0/>, which permits unrestricted use, provided the original author and source are credited.

1. Introduction

(a) La Jument lighthouse: context

Lighthouses at sea represent engineering exploits, by the challenges of the construction process, and by the extreme environmental loading they have been facing for decades or even centuries. Among these environmental forcings, the wave contribution generally dominates by far the winds or current actions on the structure. Indeed, because the lighthouses at sea are installed over shallow rocky platforms they are exposed to breaking waves responsible for intense and transient forces, also known as "slamming" impacts. During the most extreme storms, breaking waves impacts threaten the lighthouses structural integrity, which raises the question of the remaining lifetime of these fascinating monuments.

Among the endangered lighthouses at sea, La Jument, lying offshore Ushant island, Western Brittany, France (see Figure 1) is one of the most iconic. A series of pictures taken from a helicopter by Jean Guichard, showing the lighthouse keeper opening the door while a giant wave enrolls the substructure is worldwide famous. La Jument's photogenic quality is tightly related to its extreme exposition to North East Atlantic storms waves. These waves that shoal over the very steep up-wave bathymetry may violently break over the lighthouse and generate sea spray that can run up well over the lighthouse lantern (see a helicopter video record available as additional material).

La Jument was achieved in 1911 after 8 years of construction. Its erection was made possible through a generous funding provided by a C.E. Potron who requested in his testament the building of a lighthouse in the vicinity of Ushant, an Island surrounded by treacherous waters responsible for the deaths of a great number of mariners (31 wrecks were reported in the area from 1884 To 1904). The final structure, 48 m high above Chart Datum (CD), underwent, from its early years of service, worrying vibrations during the strongest winter storms. In 1911 and 1916 two storms were responsible for vibrations so intense that they caused the lantern glass to break and the mercury tank (supporting the Fresnel lens rotation) to overflow, forcing the lighthouse keepers to retrieve the toxic liquid with their bare hands ([17]). These incidents pushed the engineers to propose and perform the reinforcement and enlargement of the lighthouse substructure. This did not stop the waves to damage the lighthouse. In 1934 three holes were drilled from the substructure to 30m down to anchor La Jument directly in underlying rocky platform.

Today, La Jument keeps facing storm waves and the question of the remaining lifetime of this iconic patrimonial monument is open. The same question, applied to English rock lighthouses has recently sparks interest in the scientific community for this topic at the boundary between ocean wave physics and structural mechanics. Remarkable efforts have been conducted through the STORMLAMP project (e.g., [9, 10]) to improve the knowledge of the current mechanical response and health status of different English lighthouses exposed to high seas. Regarding La Jument, [25] has addressed the complex question of the remaining lifetime of the structure and the possible reinforcements to achieve, to extend it. His in-deep study examines the mechanical structure response to impacts of large breakers and shows that the lighthouse behaviour in terms of accelerations, displacements, strains and failures were highly correlated to the characteristics of the breaking waves hitting the lighthouse. However the knowledge of the wave field around La Jument was scarce at the time of Loraux's work and he had to rely on a wave climatology produced by a phase averaged spectral wave model to define the geometric and kinematics characteristics of the breaking waves to consider for his extreme loading cases on La Jument. He concluded that dedicated field measurements would be valuable to support his results, this statement was part of the motivation for the experiment that will be described in this paper.

(b) Lighthouses design and breaking waves

The design of any marine structure including offshore oil platforms, offshore wind turbines, breakwaters or lighthouses at sea, relies among other parameters on the knowledge of the most



Figure 1. La Jument lighthouse, Brittany France ($48^{\circ}25'20.00''\text{N}$, $5^{\circ}8'2.28''\text{W}$). Left panel: in calm wave conditions but with intense spring tide currents causing eddies in the wake of the lighthouse. The substructure added to the lighthouse to solve its early-life stability issues is well visible. Middle panel: La Jument in storm conditions. Picture courtesy of Jean Guichard. Right panel: historical plan of La Jument, before the addition of the final substructure. The current elevation of the substructure is virtually shown here (14m) as it is a key element for the paper.

extreme sea states that will possibly be faced by the structure over its lifetime. The corresponding characteristic 100 or 50-year wave is then used to compute inertia and drag forces based on Morison theory ([28]). It is now well acknowledged that in presence of breaking waves an additional impact or slamming force should be added. Indeed, at breaking onset, the horizontal fluid velocities below the free surface reach or even exceed the wave phase speed over a vertical portion of the wave crest. The wave crest (or at least part of it) behaves then as a wall of water moving at the wave crest phase speed and its encounter with a marine structure results in a violent impact, yielding a large and impulsive force. This breaking wave impact force must be considered in the marine structure design since it can be several times greater than the magnitude of the combined drag and inertia forces, though over a very short time interval ([47]). The severity of the breakers, hence the magnitude of their induced force on the structures depends on the type of breaking (e.g., [31]): the most gentle ones, known as spilling breakers are initiated by a modest jet located in the direct vicinity of the wave crests, while plunging breakers are characterized by a much more intense and large jet, enclosing an air pocket during the process. In addition, irrespective of the type of breaker the stage of the breaking process at impact is an important parameter: namely a broken wave with its highly aerated front face will cause a lower impact force than a wave at breaking onset, featuring a non-turbulent, non-aerated, vertical front face with high fluids velocities in the wave propagation direction. Why, and when waves are breaking remains an open question because the understanding of the wave breaking physics is still poor. For instance, until recently there was no consensus regarding an universal breaking onset criterion. [27] demonstrated that regular waves over a flat bottom are stable until $kH/\tanh(kd) = 0.88$, with k the wave number, H the wave height and d the water depth. In deep water, this leads to the familiar $H/L = 1/7$ threshold with $L = 2\pi/k$ the wave length of an individual wave. In shallow water Miche breaking limit becomes the so-called "breaker index" $H/d = 0.88$, while the most widely used value is 0.78 from [4]. Miche theory is not directly applicable to irregular waves propagating over a possibly varying bottom. A paper from [3] suggests that any deep or intermediate water wave with a ratio orbital velocity over phase speed greater than 0.85 will inevitably and shortly break (within a fraction of wave period). Preliminary results from [43] indicate that this breaking limit could be valid in shallow water as well. Shallow

water breaking waves have been widely studied in the literature and as mentioned above it is well known that breaking onset can be related to the breaker index H/d . [42] showed that at a given location - or equivalently water depth- the probability density function of breaking wave height was not a Dirac function but a rather broad distribution. This is due to the stochastic nature of the breaking occurrence but also probably to measurement method that detect breakers at different stage. Beyond the height of the breakers, the type of breaking controls the magnitude of the wave loads on marine structures. The well known Iribarren of surf similarity parameter ([22]), $\zeta = \tan\beta/\sqrt{S_0}$, with β the bottom slope and S_0 the deep water wave steepness, provide an empirical breaking type classification. For storm waves at La Jument, the corresponding Iribarren number takes typical values between 2 to 3 which corresponds to plunging waves according to Iribarren's classification. This is further consistent with visual observations of storms wave in the vicinity of La Jument.

Because of the associated short impulsive force, breaking waves can excite specific structural modes of marines structures including lighthouses or offshore wind turbines. For instance, [20] noted that only breaking waves were able to excite the second mode of oscillation of a 2MW fixed offshore wind turbine deployed at the Blyth wind farm (United Kingdom). [12] showed that the large remaining uncertainties in the design of offshore wind turbines are connected to our lack of knowledge of the breaking waves loading. The pioneering work from [45] assimilated the effect of a breaking wave to the impact of a cylinder falling and hitting the water. Later, [18] concluded that the breaking-induced wave on a vertical cylinder is driven by the change in momentum in the water mass drives the breaking forces. More recently, [46] proposed the following expression for the time evolution of the slamming force induced by a breaker over a vertical cylinder:

$$F(t) = \lambda\eta_b\rho_wRV^2 \left(2\pi - 2\sqrt{\frac{V}{R}}t \tanh^{-1} \sqrt{1 - \frac{V}{4R}t} \right), \quad (1.1)$$

for $0 \leq t \leq R/8V$,

$$F(t') = \lambda\eta_b\rho_wRV^2 \left(\pi\sqrt{\frac{V}{6Rt'} - \left(\frac{8V}{3R}t'\right)^{1/4}} \tanh^{-1} \sqrt{1 - \frac{V}{R}t'\sqrt{\frac{6V}{R}t'}} \right), \quad (1.2)$$

for $\frac{R}{8V} \leq t' \leq \frac{12R}{32V}$, with $t' = t - R/32V$.

The parameters are, η_b the elevation of the crest above the mean sea level, λ the curling factor that gives the height of the crest to consider for the impact the structure, V is the orbital fluid velocity in the crest, ρ_w the water density and R the radius of the cylinder. This formulation was carefully validated with a number of wave tank experiments reproducing the impact of breaking wave on cylinder and is used in design standards for offshore marine structures (see for instance: [13] for application to offshore wind turbines). Though the relevance of considering breaking waves for design purpose, the impact forces might also be considered for fatigue computations especially in shallow water environment (such as La Jument) where breaking waves are frequent ([44]). From equations 1.1 and 1.2 it is obvious that the geometric and kinematic properties of the breaking waves (i.e. the parameters η_b , λ and V) control the magnitude and time evolution of the slamming force. Also, the shape of the crest and fluid velocities inside it, vary extremely rapidly (in a fraction of wave period) preceding the breaking onset (e.g., [19]). Because of this, it is very difficult, if not impossible to infer the characteristics of the breaking waves at the moment of their impact from a typical wave climatology that provides, in the best case the frequency spectrum of the waves at several hundreds meters from the structure. This paper intends to produce a detailed analysis of the wave field around the lighthouse in storm conditions including the breaking waves that hit the lighthouse. Using waves observations synchronized to lighthouse structure acceleration measurements we will try to relate the breaking wave characteristics to the acceleration magnitude, so as to increase the understanding of the wave slamming process on lighthouses in real conditions.

(c) Objectives of the paper

In this paper we shall try to provide a finer description of the hydrodynamic condition that surrounds La Jument with a focus on the breaking waves impacting the lighthouse. The first part of the paper describes the dataset made of storm waves, current, structure acceleration observations and bathymetric data, collected from our around this lighthouse during winter 2017-18 together with additional numerical wave models output. The second part of the paper focuses on a particular storm event marked by a strong and transient acceleration peak in the lighthouse on January 3, 2018 at 9:42:07 UTC induced by a giant breaker slamming over La Jument. A discussion follows on the characteristics of this wave to elucidate why it induced considerably higher accelerations compared to the other large waves present in the same record.

2. Hydrodynamic climate around La Jument

The lighthouse is located in a macro-tidal environment. Tidal observations have been recorded in 2013 by SHOM in the Lampaul bay ($5^{\circ}06'W$, $48^{\circ}27'W$) and have been analyzed in [40]. The tidal range is 7.68 m and mean level is 4.13 m CD. Harmonic analysis on water elevation has also been computed and tidal predictions from them are used in the paper. The tidal currents around La Jument can exceeds 2 m/s and have a complex horizontal distribution (see figure 3). An analysis of the extreme conditions at La Jument has been based on the 23 years (1994-2016) of the hindcast database HOMERE ([8]). The selected point of the model is located northwest of La Jument ($48^{\circ}25'35''$ N, $5^{\circ}7'50''$ W), 1260 m away from the lighthouse. At that location the water depth is 39 m with a tidal range of 6.8 m. A blockmax method with a block duration of one month has been used to estimate the distribution of the yearly maximum. The fit on the monthly maxima by a Gumbel law gives 11.8m for a return period of 10 years. The significant wave height, H_s and current speed, C_s (only tidal current in HOMERE) are not correlated. The dominant directions of waves for $H_s > 9$ m are 250° - 300° (approximately WSW to WNW).

	Return values				most severe event*							
	10y	20y	50y	100y	H_s (m)	T_p (s)	D_p ($^{\circ}$)	U_{10} (m/s)	$U_{10,d}$ ($^{\circ}$)	C_s (m/s)	C_d ($^{\circ}$)	
H_s (m)	11.8	12.7	13.9	14.7	12.7	17	-66	21.3	-78	0.79	146	
U_{10} (m/s)	27.2	28.3	29.4	30.0	9.9	13.5	-82	29.4	-70	0.33	131	
C_s (m/s)	deterministic				large range of values						0.92	323

Table 1. Extreme Wave/Wind/Current statistics from HOMERE database, U_{10} is the 10m-high wind speed, T_p and D_p are the peak period and direction of waves, $U_{10,d}$, C_d the wind and current direction.

3. Description of the field experiment

4. La Jument experiment

(a) Context

This experiment was performed in the frame of the DiMe project dealing with the characterization of extreme breaking waves for the purpose of survivability design of Marine Renewable Energy devices such as fixed or floating wind turbines or wave energy converters. Because the observation of extreme sea states is cumbersome due to the obvious hazards faced by any instruments deployed in storms seas, little is known about their characteristics and especially regarding their breaking properties. This motivated the acquisition of oceanic storm waves observations with a focus on the breakers sub-population.

The site chosen for the study of extreme breaking sea states was La Jument lighthouse for the following reasons:

- (i) The lighthouse lies over a rocky platform that drops abruptly on its western boundary.
- (ii) The upper deck of the lighthouse is located at about 42 m above the chart datum, making possible the observation of very high sea states in intermediate to shallow waters with a large field of view and a minimal shadowing effect
- (iii) Its high location provides a (relative) shelter from the extreme sea states for onsite remote sensing instruments.
- (iv) An analysis of the HOMERE database ([8]) shows that the 10-year significant wave height at La Jument (in 50 m depth) is equal to or larger than the 100-year significant wave height of most of the French Channel and Atlantic coastline.
- (v) In the meantime a parallel experiment had been planned to measure the acceleration of the lighthouse under storm waves impacts, based on the recommendations of [25].

The connection between the initial storm waves study and the acceleration measurements appeared to be relevant and motivated the writing of the present paper.

(b) Instrumental setup

The deployment of an X-band radar, stereo-video system and four accelerometers on La Jument took place on December 5 and 6 2017. Because the access to the lighthouse by sea is hazardous, especially in winter, we relied on the civilian security helicopter to reach La Jument. Previously, a wave buoy and a current profiler were moored in the winter by Shom to yield independent information regarding offshore wave field and current vertical profile. Finally, a bathymetric survey was performed in July 2018 to improve the knowledge of the water depth around the lighthouse. The next section will be dedicated to a description of the instruments involved in this field experiment.

(i) In situ instruments

(ii) Stereo video system

The stereo-video cameras are mounted on each side of a hut located just below the lantern and looking approximately 246° N. The stereo video system used in this experiment consists in a pair of synchronized 5 Megapixel (2048x2456 pixels) BM-500GE JAI cameras, with 5 mm and wide angle lens. The configuration of the lighthouse imposed a maximum camera separation (baseline) of 5.44 m. The stereo images acquisition rate were set at 10 Hz and time stamped thank to a GPS time server. The camera are at about 42 m above the chart datum and are equipped with sprinklers and wipers enabling to clean them before each acquisition and during extreme sea states conditions. This system has enabled to collect 7 TB of storm waves, corresponding to about 35 hours of observations collected between December 6, 2017 and January 15 with significant wave height reaching 10.5 m in the area of the lighthouse. The sea surface reconstruction method used here follows the same principles presented by [5] and [23] and use the WASS (Waves Acquisition Stereo System) code version 1.4, from [6].

The sea surface area covered by the stereo video images and the surface resolution mostly depends on the experimental setup, local brightness and sea level position. The expected accuracy of the stereo observations has been derived using the formulations of the quantization error [34]. For the stereo setup used to here, the expected quantization error is represented by the root-mean-square (*RMS*) errors along the *x*-, *y*-, and *z*-axis.

This set-up allowed to capture the wave field at 50 m from the foot of the tower up to 250 m offshore, with a $RMS_x = 0.14$ m, $RMS_y = 0.35$ m and $RMS_z = 0.09$ m, with a local absolute maximum error of 28 cm for the furthest elevation points. With that set-up we were enables

to capture the intense wave shoaling and possible breaking occurring in the vicinity of the lighthouse.

The main source of error observed in the system was related to the correlation around the breaking events. Breaking waves form bright patches over darker surface water, some times resulting in strong brightness gradients and strongly disturbs matching processing. The correlation around the foam patches was improved by [23], however this still one of the main restriction in the stereo video reconstruction, especially over the large breaking waves in front of the lighthouse. Therefore the analysis of the wave field in the direct vicinity of the lighthouse was performed with extra care because of the presence of larger breakers.

(iii) X-band marine radar

All radar data used within this study were acquired by a 12 kW marine radar, operating at X-band (9.3 GHz) with vertical polarization in transmit and receive (VV-pol). The radar was mounted at a height of ~ 43 m above mean sea level and run in a rotational mode covering a range of ~ 3260 m at ~ 0.5 Hz around the light house (orange dotted circle in Figure 2). The radar was operated with a pulse length of 50 ns, which resulted in a range resolution of 7.5 m. The antenna had a vertical beam opening of 21° and a width of 7.5 feet (2.3 m) resulting in an azimuthal resolution of $\sim 0.9^\circ$. The radar was run with a pulse repetition frequency of 2 kHz and the backscattered signal was run through a linear amplifier and then digitized with 13 bit.

Within this experiment the X-band marine radar is being utilized to observe ocean waves in space and time. This allows to measure the 2D wave spectra from which parameters such as the peak wave direction and peak wave period can be determined [7], [11]. In addition the radar data allow to measure surface wave properties such as wavelength and phase velocity, which in turn enable to retrieve the surface current vector [39], [21]. The surface currents result from the difference of the observed phase velocity to that given by the linear dispersion relation of surface gravity waves, which is given by

$$\omega = \bar{\omega}(\mathbf{k}) = \sqrt{gk \tanh(kd)} + \mathbf{k} \cdot \mathbf{U} = \bar{\omega}_0(\mathbf{k}) + \mathbf{k} \cdot \mathbf{U} \quad (4.1)$$

where \mathbf{k} is the wave number vector, g the gravitational force, d the water depth and \mathbf{U} the two-dimensional near-surface current. A detailed description of the methodology utilized in this study to extract the surface current fields is described in Streßer et al. [41]. An in depth validation of marine radar retrieved surface currents to surface drifter measurements has shown a root mean square error of < 0.04 m/s [26].

(iv) Accelerometers

The 4 accelerometers RECOVIB-IAC-A03 were firmly mechanically fixed on the lighthouse at four different heights: 20.6, 31.1, 38.7 and 45.6 m above the chart datum. The highest one is mounted on the steel structure that supports the lense close to the top of the lighthouse while the 3 remaining are directly tightened to the rocks of the wall. These accelerometers are able to measure accelerations in the range $\pm 2g$ (with g the gravity acceleration) giving out a current from 4-20 mA. They embed a low-pass filter of 1st order of with an upper frequency limit of 1000 Hz (-3dB). The accelerometers are wired to a data acquisition system which is independent of the one used for Radar and Cameras but synchronization with the wave observations was possible thanks to a GPS time stamping. The power consumption of this systems is very low compared to the other devices deployed for the experimentation so that is possible to record all the data along the winter even not stormy periods. The data acquired at 5 KHz, were stored in the lighthouse in a dedicated hard drive and transferred on an hourly basis to earth to allow preliminary analyses of the data without physical access to the lighthouse.

(v) Bathymetric campaign

The physiography of the areas is poorly known. Bathymetry data is typically scarce in nearshore areas because of high operating costs associated with time-intensive hydrographic surveys with echosounders (as the width of the swath covered by the acoustic fan of the echosounder reduces with water depth) and difficulty of navigation in shallow, uncharted waters. Airborne bathymetric LIDAR techniques now allows filling this gap in the nearshore. The Litto3D® program ([30] ; [15]) provides extensive bathymetric coverage of coastal waters in Western Brittany, and in particular in the nearby Molene Archipelago ([16]). Still, bathymetric information was lacking in immediate vicinity of the Jument, while it is critical for fine-scale understanding and modeling of wave propagation and wave breaking. Water depth around the lighthouse is beyond bathymetric lidar capabilities due to the steep seabed slope near the lighthouse, and the strong tidal currents and high waves make this zone of rocky shoals very difficult to marine navigation (numerous shipwrecks). This motivated a field campaign in July 2018, conducted with the research vessel (R/V) "Albert Lucas", to collect the bathymetry data over an area of a few kilometer squared around La Jument. The hydrographic survey was carried out with a shallow-water multibeam echosounder (MBES) Kongsberg EM3002 (high-resolution 300 kHz MBES system) coupled with a hull sound velocity sensor (H-SVS) Valeport miniSVS, an inertial measurement unit (IMU) IxSea Octans3000 and a global navigation satellite system (GNSS) Astech ProFlex500. Sound velocity profiles (SVP) were carried out with an AML BaseX equipped with SV and P Xchange sensors. The GNSS navigation was processed according to the post processed kinematic (PPK) method with Novatel GrafNav software and the multibeam soundings were edited with QINSy software, in order to provide a 2-m grid DTM.

(vi) Additional in-situ measurements

To complete the field campaign, one waverider buoy (Datawell) and an acoustic wave and current profiler (AWAC) were deployed in front of the lighthouse.

The buoy was located about 3 km away from the lighthouse ($5^{\circ}10.410'W$, $48^{\circ}25.131'N$) in the western direction, at the limit of the radar coverage (see figure 2). The buoy was deployed on the November 27, 2017 and recorded until March 3, 2018. It provided the wave spectra every 30 minutes from which integrated wave parameters have been extracted.

The current profiler was deployed about 300 m away from the lighthouse ($5^{\circ}08.196'W$, $48^{\circ}25.284'N$) in the south-western direction, at the limit of the video-system reconstruction area (see figure 2). Moored with the buoy on the November 27, 2017, the AWAC stopped its acquisition on the February 1, 2018 and was found strongly damaged on the inter-tidal area on the north of Ushant island two months later. The analysis of the data revealed that the instrument was not stable on the bottom and the instrument records showed a tilt up to 40 degrees due to ebb currents. A strong filtering have so been applied on the data to keep only the data acquired in the validity range given by the instrument constructor. As a results, more than 60% of the AWAC observation bursts have been removed, mainly during ebb tides.

5. Results

(a) Observations

(i) Bathymetry

Figure 2 shows the bathymetry surrounding La Jument. The lighthouse stands on a promontory that is always submerged except during low spring tides, at the Western extremity of the southern underwater ridge extending to the West from Ouessant Island. Such setting will tend to focus energy on the promontory due to wave refraction as will be shown below with ray tracing study. This particular relief is inherited from the regional-scale structural deformation of the bedrock, with a series of East-West trending faults (Ehrhold et al., 2017) including the North-Ouessant

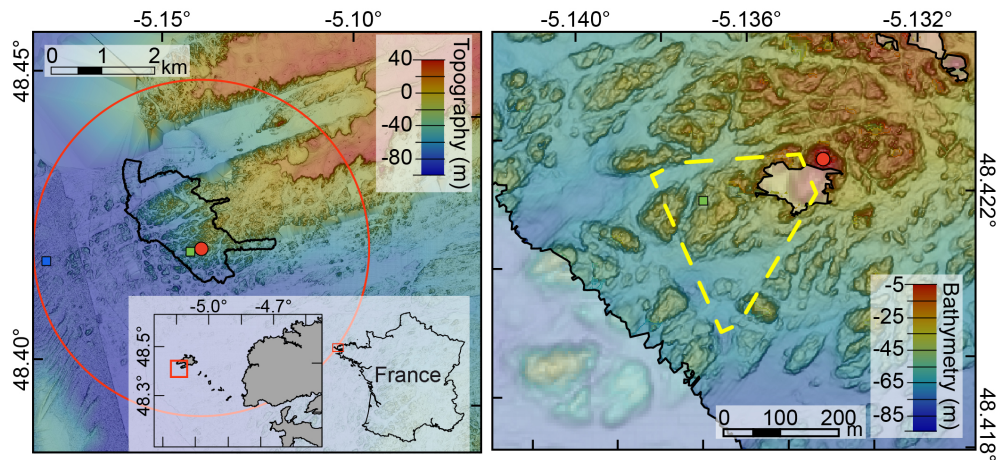


Figure 2. Bathymetry around La Jument. Left panel: global view, La Jument position is marked the red dot. The blue (green) square displays the location of the wave buoy (AWAC). The red circle indicates the domain covered by the X-band radar. The bold black line shows the area covered by the bathymetric survey conducted in the project. Right panel: zoom on La Jument bathymetry. The green square is the AWAC position and the the dashed yellow line encloses the stereo video reconstruction domain. The blurred area corresponds to pre-existing bathymetric data.

fault, yielding significant topographic steps across these faults. Our high-resolution bathymetry reveals with greater details the densely-fractured bedrock on the barren platform that is extending 2 to 3 km away to the west and south of the lighthouse. Except for the area north of the Jument, in the fault-controlled depression creating an embayment in the western coastline of Ouessant and where the bathymetry is smooth, as well as in the bedrock fractures, there is no sediment cover on the granitic bedrock, consistent with high-energy hydrodynamic conditions. Secondary fractures also occur oblique to the main fault orientation. The dense network of fractures yields a rather chaotic seabed relief with large blocks separated by deep incisions. The waves that we will describe in the rest of the paper are propagating approximately from WNW, hence will advance towards the lighthouse over this indented topography that will affect their properties. The bathymetry data collected here are therefore of primary importance when examining the wave physical processes (refraction, shoaling and breaking) that will control wave loads on La Jument.

(ii) *in situ* measurements: current profilers and wave buoy

(iii) X-band radar observations

The marine radar retrieved current fields from January 3, 2018 between 0815 and 1030 UTC are shown in Figure 3. Each current map results from approximately 15 minutes of radar data. The window size for the retrieval of each current vector is 480×480 m and adjacent cells are overlapping by 50%, which leads to one current vector every 240 m. For the current field retrieval only wave lengths between 15 and 100 m were considered, which approximates the mean current in the upper 7 m. Figure 3, shows the current field at different instants close to the time of the waves and accelerations record that is discuss in detail in the rest of the paper. It shows a complex horizontal distribution of the current field with velocity magnitude reaching 1.8 m/s over the domain of interest and about 1m/s in the vicinity of La Jument at the time (09:47:30 UTC, third panel of figure 3) close to the wave event considered in the rest of the paper.

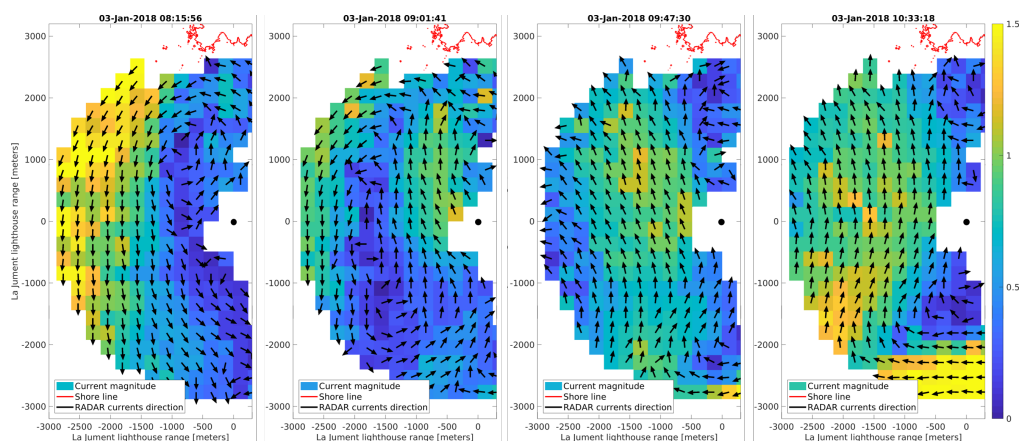


Figure 3. Marine radar retrieved current maps of January 3, 2019 between 0815 and 1030 UTC (left to right). The color coding gives the current magnitude and the unit vectors represent the current directions. Each map was generated from 15 minutes of marine radar data.

(iv) Stereo video observations

Between December 2017 to March 2018 several storm events were significant wave height (H_s) ranging between from 7.5 to 10.5 m. A summary of the main wave parameters captured by the stereo video cameras during those days is presented in the table (iv).

Date	H_s [m]	T_p [s]	D_p [°]	C_s [m/s]	U_{10} [m/s]
03/01/2018 09:39	10.03	13.3	279	0.77	17.9, W
03/01/2018 10:30	10.51	15.4	278	0.69	15.5, W
03/01/2018 11:09	8.33	12.5	282	0.36	15.5, W
03/01/2018 11:54	9.63	12.5	281	1.08	15.5, W
04/01/2018 09:40	7.34	11.1	279	0.65	15.0, W
04/01/2018 10:45	7.18	10.5	286	0.79	14.7, W
04/01/2018 11:43	7.52	11.1	274	0.52	14.7, W

Table 2. Summary of the main storm event recorded by the stereo video system in winter of 2017/2018. The date mark the time that the stereo video acquisition starts. The significant wave height (H_s) and peak wave period (T_p) for each event is measured by the stereo video system, the peak wave direction (D_p) is presented at the Datawell location (without the bathymetry effect), the mean current speed C_s is measured from the x-band radar and the wind speed at 10 m height (U_{10}) is estimated from the European Centre for Medium-Range Weather Forecasts (ECMWF).

Several breaking waves over 15 m (from crest-to-trough) were recorded in front of our cameras, and the largest wave observed was 23.6 m high about 200m to the WSW of the lighthouse. An example of extreme breaking wave (19 m high) captured by the cameras is presented at figure (iv) where the a extreme wave "runup" reaches more than 42 m blinding the cameras lenses.

(v) Accelerometer observations

The purpose of our experiment was to investigate the relation between the incoming wave field and the mechanical loading felt by the tower in a wave-by-wave framework. To achieve this, we have focused our efforts toward a deterministic comparisons of the waves captured by our stereo system and of the wave-synchronized accelerations measured inside the lighthouse. Because of the slender geometry of the lighthouse, the accelerations induced by waves are larger at the top

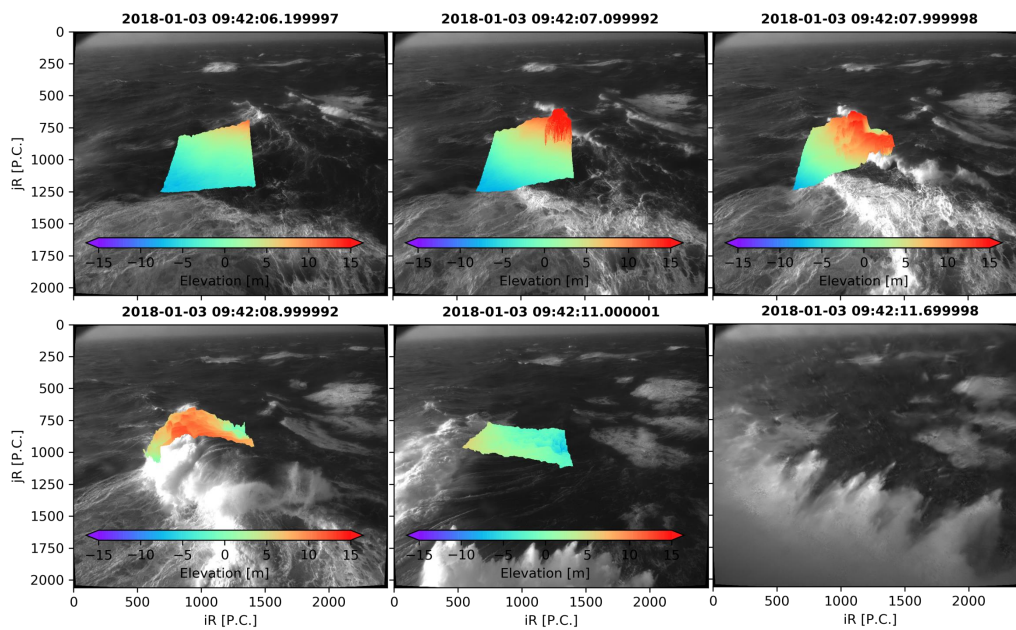


Figure 4. Examples of stereo video 3D surface elevation map $z(iR, jR, t)$ plot over its correspondent right camera bitmap image in the pixel reference system. The sequence of images shows an extreme breaking event (corresponding wave height: 19.0 m) where the vertical water excursion washed the stereo video cameras at ~ 42 m

than at the foot of the lighthouse hence the ratio signal-to-noise ratio of the highest accelerometer is more favorable to examine the effect of waves on La Jument mechanical response. Figure 5 presents the samples of accelerations that were collected on January 3 between 08:00:09 and 12:59:29 UTC, containing x or y -acceleration with absolute values above 2m/s^2 .

Only four impact events satisfying this condition were found. A careful examination of the acceleration records before any magnitude-filtering reveals that these acceleration peaks are isolated and easily identifiable above a background noise of about 0.16m/s^2 standard deviation. These features are also evident on the left panels of figure 5. The zoom of the accelerations bursts shows strong oscillatory accelerations in the two horizontal directions that vanishes after a few seconds. Interestingly the maximum of accelerations is along the x -axis for the first and more intense event and along the y -axis for the three remaining events. This indicates that the breaking waves may impact the lighthouse from different angles. More details regarding the accelerations and the mechanical response of the lighthouse to wave induced loads can be found in [14] for the interested reader. In the present paper we simply use the horizontal acceleration peaks as a proxy for the severity of the wave impacts. We shall then explore the characteristics of the waves that caused these sporadic, isolated, and intense accelerations events to elucidate what sets them apart from the rest of the wave population so as to progress in the understanding of the causality between waves and structural damages to lighthouses. Our investigations will focus on the acceleration event of January 3, 2018 at 09:42:07 UTC displayed in the two first panels of figure 5. Our choice was guided by the magnitude of the acceleration felt by La Jument (the largest recorded in our analysis) but also by the quality of the available synchronized reconstructed surfaces.

(b) Modeling

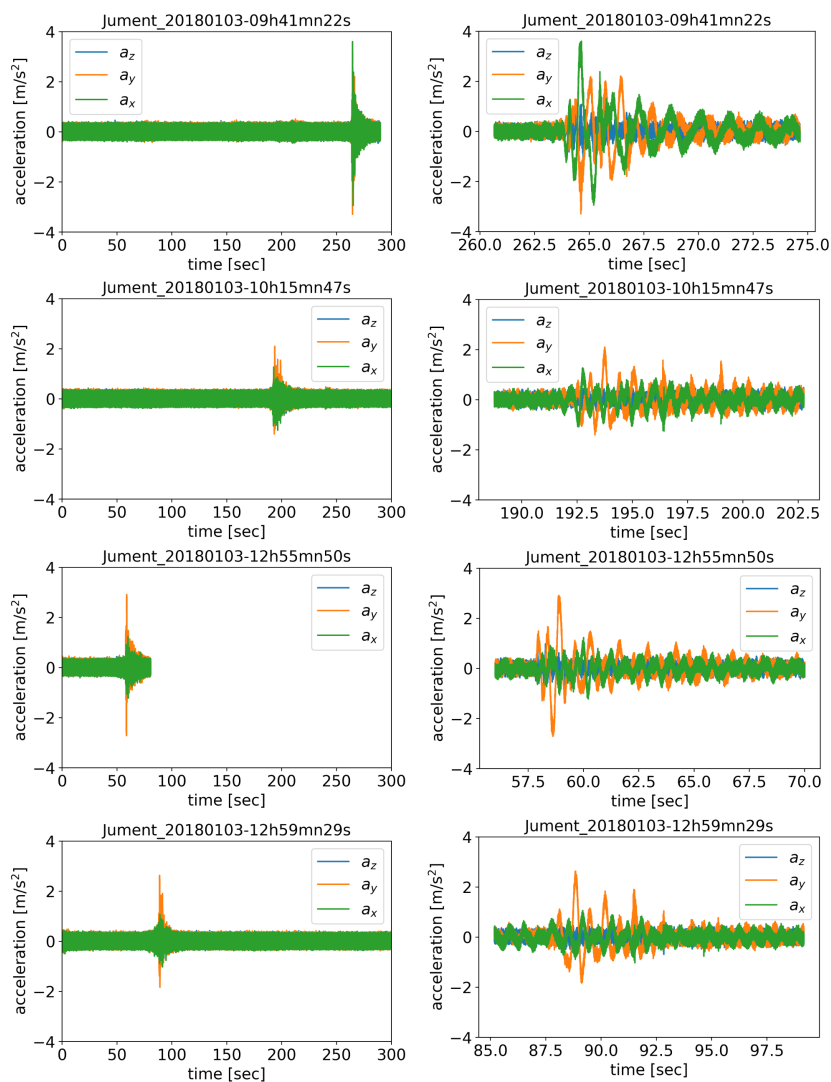


Figure 5. Samples of acceleration collected by accelerometer 4 (highest sensor) over 3 axis: x , y , z . Only samples showing acceleration magnitude in the x -axis over 2m/s^2 and with available stereo-video observations are presented here. The vertical acceleration a_z has been reduced by the local gravity g .

(i) Wave propagation toward La Jument

The comparison between significant wave heights observed at buoy DW and wave current profiler AWAC are displayed on figure 6 for the sea states with peak wave direction coming from west ($250^\circ < \theta_p < 290^\circ$). The figure 6 shows a non linear relationship of significant wave heights between the two locations and can not be only related to the shoaling induced by the water depth. Then the wave propagation from the buoy to the lighthouse is expected to be a complex combination of wave-bathymetry and wave-current interaction.

To investigate the wave propagation from the offshore buoy DW to the lighthouse and further understand the wave transformation toward the lighthouse, we used a simple wave ray model. The sea state is simplified to a single Airy wave, with the period (resp. direction) corresponding to the observed peak wave period (resp. direction) at DW. The amplitude of the Airy wave is defined to fit the observed significant wave height. Then, a long crest is created on each side of

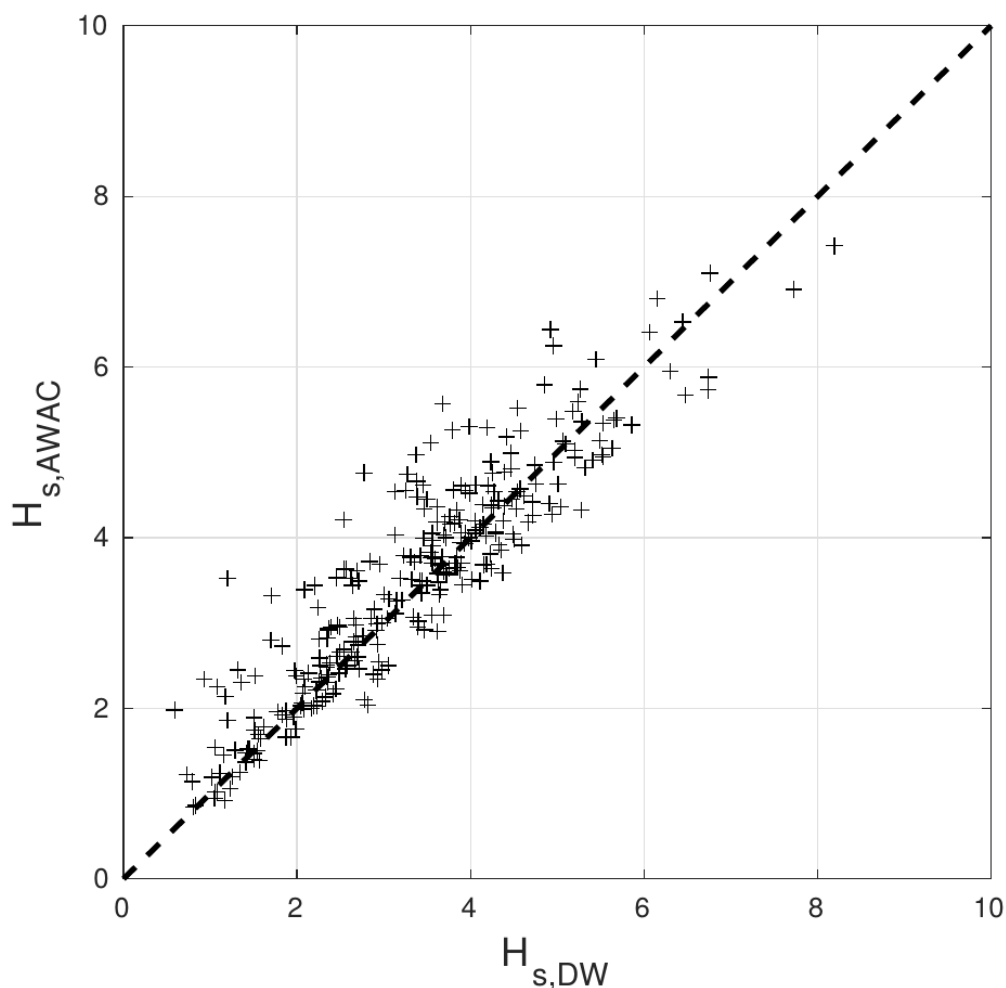


Figure 6. Comparison of significant wave height (in meters) observed at the buoy and at the AWAC.

the buoy and discretized each 2 m. The wave rays and the wave amplitude along each ray are then computed, following Airy theory, with and without currents at each stereo video acquisition dates. The obtained amplitudes are then converted into significant wave height. The currents used in this section are simulated by the MARS model implemented on the Iroise Sea at a resolution of 250 m ([2]). The results of wave ray tracing are shown on the figure 7 and obtained significant wave height at AWAC location and in the stereo reconstruction area are given in table 3.

Despite the obvious limitation of this approach, the impact of currents on wave propagation is clearly shown (see figure 7 and table 3). Moreover, range of significant wave height obtained in stereo reconstruction area are in line with the significant wave heights computed from stereo video system. Nevertheless, we must note that the wave field observed by the stereo system is strongly non-homogeneous with up to 3 m difference of H_s in the reconstruction area.

(ii) Phase resolving wave modeling

BOSZ is a phase-resolving Boussinesq-type model for the computation of nearshore waves, wave-driven currents, infra-gravity oscillations, ship wakes waves, and near-field tsunamis (see for example [37], [36], [35], [24]). The governing equations are based on a conserved variable formulation of [29]. The solution structure covers the nonlinear shallow water part of the

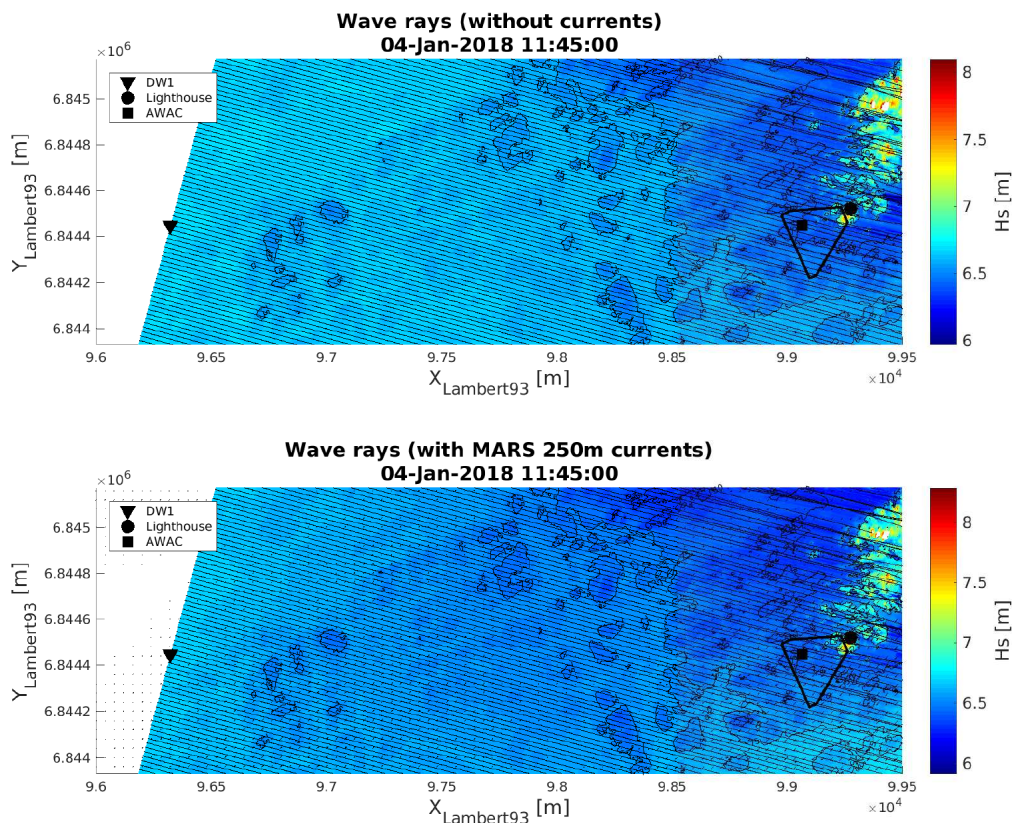


Figure 7. Example of significant wave height map obtained with wave ray tracing for event on 04/01/2018 11:45. Black lines are the computed wave rays (1 over 10 rays are plotted). Top panel consider only wave-bathymetry interactions (water elevation obtained from predictions at Lampaul harbour), bottom panel also consider wave-currents interactions.

Date	$H_{s,DW}$ [m]	$H_{s,AWAC}$ [m]	$H_{s,STEREOAREA}$ [m]
03/01/2018 09:45	9.48	9.58 (9.71)	9.05 - 11.92 (9.14 - 12.23)
03/01/2018 10:30	10.41	10.13 (9.88)	9.65 - 12.13 (9.50 - 11.86)
03/01/2018 11:15	8.75	9.23 (9.39)	8.83 - 12.05 (8.95 - 12.35)
03/01/2018 12:00	5.64	5.95 (6.28)	5.68 - 7.56 (5.96 - 8.54)
04/01/2018 09:45	4.10	3.96 (4.27)	3.91 - 4.62 (4.18 - 5.12)
04/01/2018 10:45	5.69	5.62 (5.71)	5.43 - 6.83 (5.45 - 6.95)
04/01/2018 11:45	6.67	6.40 (6.41)	6.19 - 7.54 (6.23 - 7.63)

Table 3. Table of resulting significant wave height obtained with wave ray tracing. $H_{s,DW}$ is the significant wave height observed at buoy DW1, $H_{s,AWAC}$ is the significant wave height obtained with wave ray tracing at AWAC location and $H_{s,STEREOAREA}$ is the range of obtained significant wave height in the stereo reconstruction area. Values out of parenthesis are values obtained without currents, whereas values in parenthesis are obtained considering MARS 250m currents.

governing equations with a Finite Volume scheme based on a total variation diminishing (TVD) reconstruction method of up to 5th order and a HLLC Riemann solver. This ensures robust and accurate computations of fast flows over irregular terrain including wet/dry boundaries. The frequency dispersion terms are based on a central-differential Finite Difference scheme. The

time integration is carried out with Runge-Kutta schemes of up to 4th order and adaptive time stepping. Animation of the wave transformation in the vicinity of the lighthouse are available as additional material.

The computation of the wave field around the lighthouse of La Jument is based on 2.7 km by 2.5 km domain composed of a cartesian grid of uniform 7.5m by 7.5m. The input wave spectrum comes from a Datawell observation at Jan 3, 2017 at 9:30AM. The significant wave height is 9.74 m and T_p is 13.3 sec. The peak direction is almost perfectly west (280 degrees) and the directional spreading is narrow with 90% of the energy around ± 25 degrees from the peak. The BOSZ computation was carried out for 1h and 20 min with the first 20 min used for wrapping up the solution. The water level offshore was truncated to 91.2m depth (including tide level) to ensure validity of the input spectrum. The wave field shows strong convergence in close proximity to the lighthouse with H_s values 50% higher than the observed offshore conditions.

(c) Focus on one extreme slamming wave

The analysis of the accelerations record of January 3, 2018, revealed that the occurrence of one particular wave event impact occurring at 9:42:07 UTC, caused a peak several times higher than the second most intense acceleration. Fortunately at this time, the stereo-video system was running and able to capture the wave responsible for the acceleration peak. Video images shows a water vertical excursion consecutive to the wave slamming on the lighthouse that washed up the video cameras located about 41 m above the sea level (at that instant). This wave is illustrated by Figure iv showing the evolution of the wave toward and during the breaking process. Unfortunately the stereo-video images do not give access to the impact zone of the wave on the structure as the video images do not cover the foot of the lighthouse and because the white waters in the immediate vicinity of the lighthouse make stereo reconstruction inaccurate. A careful visual analysis of the other video records revealed that no other wave caused such water runoff. In the following we will explore the characteristic of this wave, referred to as "wave1" from now on, just before it impacts La Jument.

(i) Stereo-video analysis

(ii) Spatial wave properties analysis

We shall here use a combination of the video images and of the stereo-video reconstruction to obtain a better description of the high waves of interest at the foot of the breakwater. The strength of the stereo-video system compared to other traditional point *in situ* wave instruments is of course its ability in providing spatio-temporal information on the wave field. Indeed, if the relation between space and time is well described by [1]'s linear theory for small amplitude waves, the same theory would fail if applied to our irregular large amplitude waves nonlinearly distorted by their interaction with the sea bottom. Figures 8 and 9 display snapshots of the sea surface capturing the spatial signature of the 8 waves, with crest higher than 8 m above the mean sea level, at the inner edge of the stereo domain (closest location from the lighthouse). We chose to select our subset of high waves based on their crest elevation, instead of their trough to crest height because it seems that the elevation of the crest impact on a marine structure is a key parameter in the impact on a marine structure as evident in the impact force formula of [46] (see equations 1.1 and 1.2). The photographs of these waves (figures 8 and 9, left panels) indicate that they were all breaking at the foot of the lighthouse. Compared to the others, wave1 appears to have strong variation of the along crest elevation, with high elevations concentrated close to the lighthouse. Snapshots of wave1 nonlinear evolution toward breaking is available in Figure iv, and animations of the wave surfaces overlaid over the video images can be analyzed to further understand the breaking process at the foot of the lighthouse (these videos are available as supplementary material, note that the reconstruction area has been reduced in these video to highlights the breaking areas). It reveals that when the wave crest is approaching the structure a fast flow toward the crest appears and seems to be associated with the birth a secondary jet just

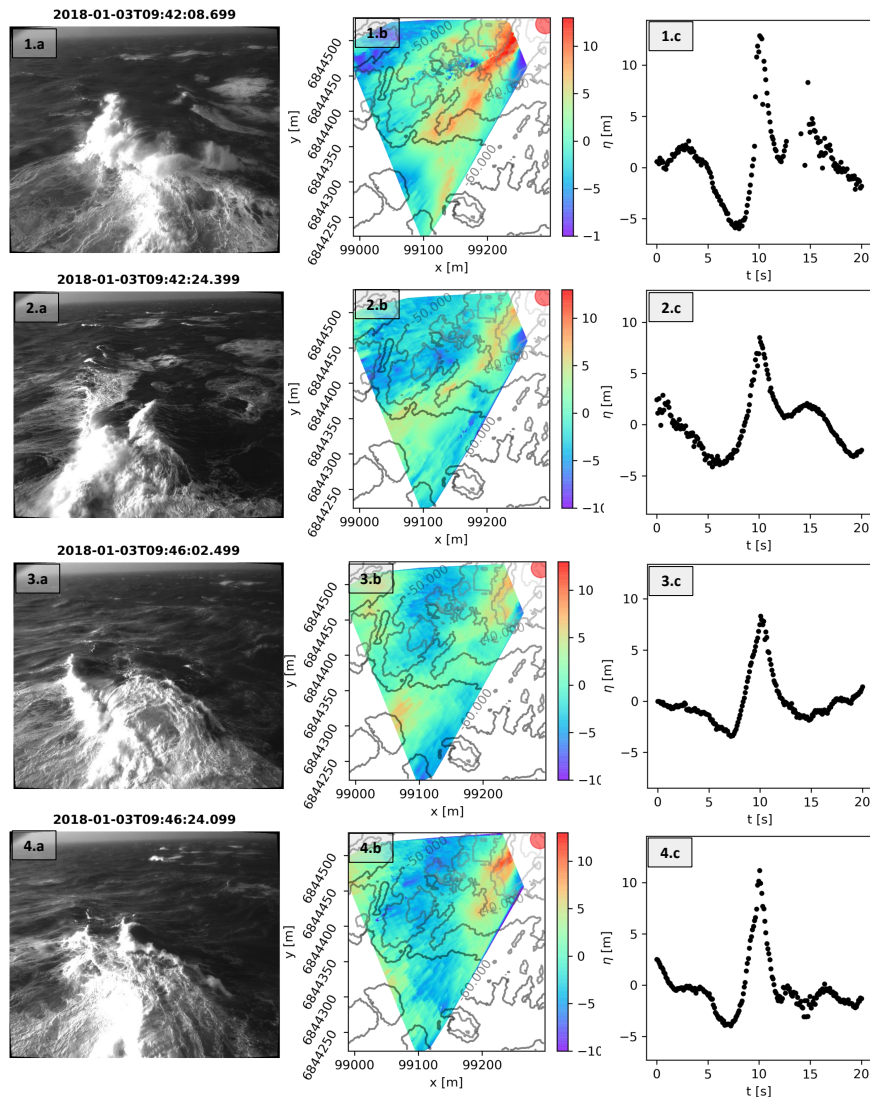


Figure 8. Description of the 8 high waves selected for our study (4 in this Figure and 4 in figure 9). Left panels: video images, middle panel reconstructed wave surfaces projected in a Lambert93 geographic system overlaid over iso-contours of water depths, right panels: time series of the high waves elevation, collected at $x=99250\text{m}$, $y=6844500\text{m}$ from the stereo video reconstruction.

below the main crest. Finally both crests merged into one that violently overturns. This feature resembles the "bazooka effect" put in evidence by [38], in highly energetic breaking waves. The figure 9.6.a also shows a good illustration of the secondary jet generation.

(iii) Time series analysis

We analyzed the same surface by extracting a 30 min time series of the sea surface elevation recorded by at a single point located at the closest possible location from the lighthouse ($X=99250\text{m}$, $Y=6844500\text{m}$ in the stereo images of Figures 8 and 9, for an acquisition starting at 09:39:38 UTC. With this record, we pursue our investigations of the properties of our high waves subset. Superposing the individual waves on a single plot shows time profile similarities between the 8 high waves selected. Some of the characteristics of these waves are listed in table 4.

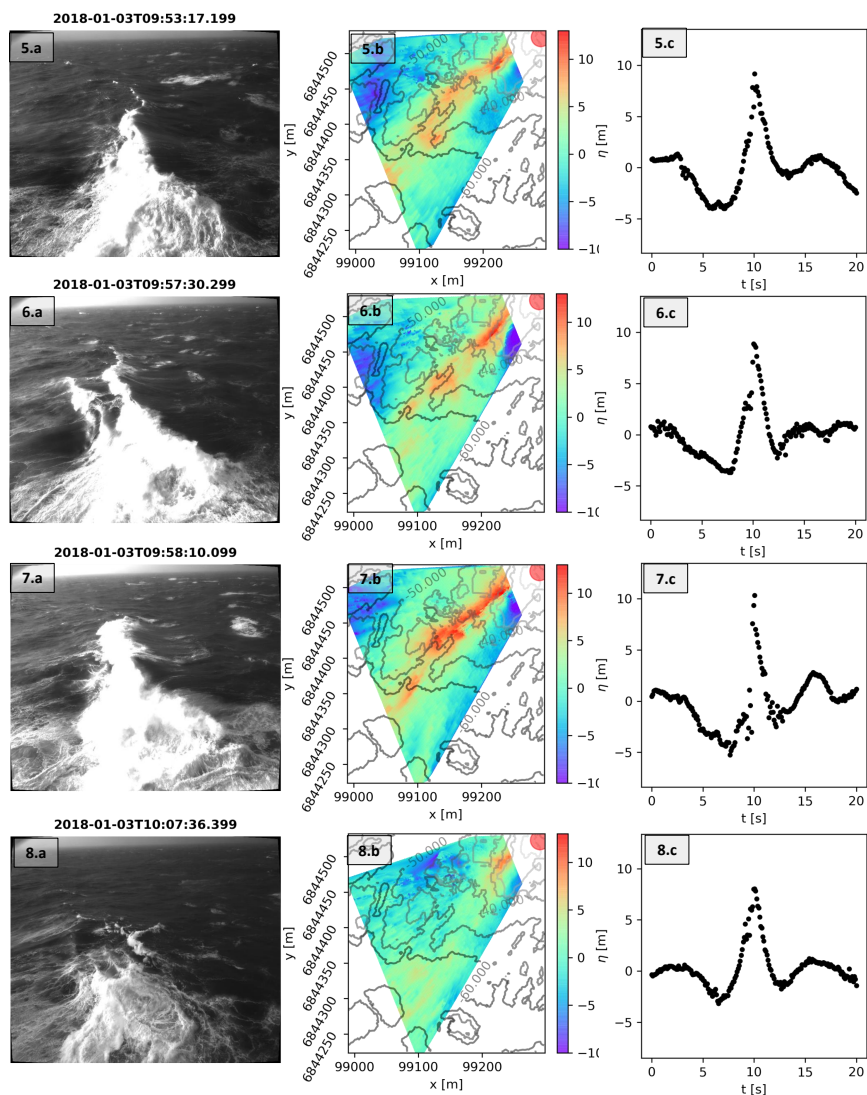


Figure 9. Same as figure 8 but for the four remaining high waves.

Table 4. Crest and trough elevation, wave height, and half period (duration between front trough and crest) for the 8 high breakers studied in the paper.

wave no	η_c [m]	η_t [s]	H [m]	$T_{1/2}$ [s]
1	12.9	-6.1	19.0	2.0
2	8.5	-4.1	12.6	4.6
3	8.3	-3.4	11.7	2.9
4	11.2	-4.0	15.2	2.8
5	9.2	-4.0	13.2	2.9
6	8.9	-3.7	12.6	2.2
7	10.3	-5.3	15.6	2.4
8	8.0	-3.2	11.2	3.5

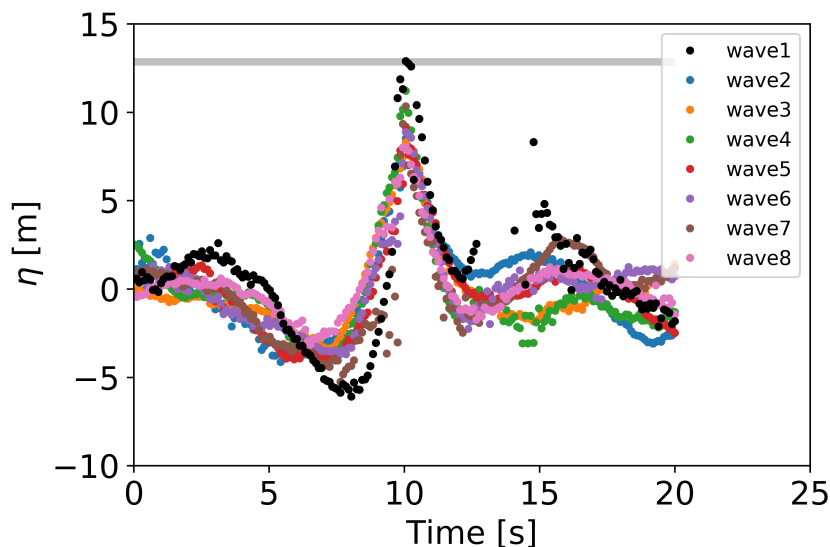


Figure 10. Comparison between wave1 (black) and the 7 other high waves for the record of January 3, 2018 at 9:39 UTC. The grey bar indicated the altitude of the lighthouse substructure (see figure 1) above the sea level at the time of the wave record. The vertical extent of the bar corresponds to the water level change over the 30 min of the record.

Such similarities in the wave profile of high waves was already discussed for deep water waves by [32] and [33] who proved that for Gaussian sea states, the highest waves profile were in homothety with the auto-correlation function of the full wave field. Our wave are all skewed, the crests being much higher than the troughs and asymmetric, the front face being significantly steeper than the back face. Most of them are followed by a secondary crest. Table 4 and figure 10 demonstrate that wave1 has the highest crest (12.9 m) with a shallow preceding trough (-6.1m) and the largest individual wave height (19.0 m). The second highest wave (wave7) has a wave height reach 15.6 m but with a deeper wave trough (-5.3 m) and lower crest (10.3 m) than wave1. At the studied location, which is not exactly at the foot of the lighthouse, the time separating the preceding trough and the crest of wave1, which can be linked to the front face geometric steepness is only 2.0 s which is the lowest value among the different waves, though other waves seems to be very steep as well. We note also that the record of the back trough of wave1 is dominated by noise because of the water spray induced by the wave slamming that blinded the video cameras and corrupted the reconstruction for a short period of time. On figure 10 the grey bar indicates the elevation of the top of the lighthouse substructure, the bar thickness translates the water level variation over the time period of the wave record, namely the water level dropped from 42cm during the 30 min wave record considered. We note that the water level used here ([40]) do not take into account storm surge effects which likely results in a slight overestimation of the elevation of the substructure top (the grey bar in figure 10 would likely slightly lower with storm surge accounted for). Figure 10 indicates that the crest elevation of wave1 is the only one crossing the substructure elevation level. We advance that this is a plausible explanation for the acceleration peak found for wave1 only. Since La Jument's tower is much more flexible than the substructure itself ([25]) the mechanical response to wave slamming impacts on the tower is significantly more intense and translate into much larger accelerations than those due to waves impacting the substructure only. This would explain while waves with slightly lowest crest elevations, such as wave7 did not cause any vibrations on the structure. Of course, it is difficult to be fully conclusive regarding the actual elevation of the crest right at the lighthouse, from considerations derived from observations collected at 50m away from the structure.

Fortunately, a series of pictures of wave1 taken from Ushant Island supports our findings. These improbable but highly valuable pictures are available in [14] and presents the detail of wave1 impact on La Jument (*for the review stage, a picture is available as additional material*). Two elements match to relate the pictures to wave1: the correspondence of the time stamps is less than 2 min (probably to inaccuracies in the camera clock) and wave1 was the only wave in our records of the day that caused water spray up to the stereo-system.

From this detailed study of our high waves subset, we conclude here that the crest elevation relative to the altitude of the substructure top is a key parameter to consider in the damage studies on La Jument.

6. Discussion

The paper introduces a broad spectra of observational and model data that we have used to provide a better understanding of the complex hydrodynamics that surrounds La Jument. However, the coming discussion will focus on the wave-acceleration study performed in the previous section.

The first analysis presented here focused on the examination of a particular stereo-video record featuring an large breaker that induced significant horizontal accelerations in the tower and caused water spray that reached up to the video cameras. As said in introduction, the mechanical response of La Jument under extreme waves was addressed in detail by [25] who simulated the loading of a series of three waves with characteristics based on the estimation of 50 to 100-year return period waves, combined with varying tidal level. The horizontal acceleration caused by wave1 (looking at the x -axis) is of the same order or magnitude as the values report by Loraux's numerical experiment, though his largest numerical wave (22m high with crest elevation of 18 m) combined with a 8.5m CD tidal level, (50 cm above the highest astronomic tide and 6.5 m below the substructure top) yields an horizontal acceleration peak above 20 m/s^2 . We should here stress that the waves studied in our paper correspond to a severe but not extreme storm : indeed the significant wave height of 10.5 m is only 2-year return period event. In addition, the tide level was low (1.15 m CD in average over the 30 min record) which places the water level 12.85m below the top of the lighthouse substructure. Even in these "adverse" conditions, our instruments captured a wave able to hit the lighthouse's upper tower causing important vibrations (double integration in time yields horizontal displacements of about 5 mm at the top of La Jument). One of the key to explain this finding, it that oppositely to Loraux we consider waves individually and of course some of them can be higher that the significant wave height, indeed wave1 is 19 m high. Individual waves in 50 or 100-year storms can then possibly be even (much) higher than that consider in [25], even though the breaking process may limit the incoming wave height at some point. This advocates for more observations in stronger sea states with different water levels to accumulate more accelerations data synchronized to wave observations. This would further help understanding the relation between the wave characteristics in term of wave height, period and direction, the water level and the tidal currents on the impact strengths on the structure. Also a larger subset of high waves reaching the tower would be necessary to examine what other properties (e.g., breaking type, breaking stage, angle of attack, fluid velocities in the crest) are important, beyond the crest elevation. In addition, since the stereo-video domain does not cover the last 50 m of wave propagation and transformation before impact, efforts with numerical models able to represent the 3D geometry and fluid velocities of the crest would help in the cross interpretation of the wave characteristics, (that we have sum up to the crest elevation only here), with an appropriate numerical model. Especially, this would yield valuable information regarding the type of breaking wave and the stage of the breaking process which are important parameters in the estimation of the slamming pressures.

As said previously, except wave1, no other wave in the 30 min record analyzed produced a detectable acceleration, while we verified that several other large waves (8 with wave crests higher than 8m at 50m away from La Jument) broke at the foot of the breakwater. This finding confirms the numerical results of Loraux who reported that breaker impacts on the substructure

only, do not produce any significant accelerations on La Jument (see figure 46 in Loraux's study). The substructure built several years after the lighthouse erection plays therefore a double role: it adds stiffness to the initial lighthouse tower and protects it from the assaults of most of the breaking waves, except in storm conditions and high tide levels.

The accelerations records have only been briefly addressed in the paper and served just as markers of the wave slamming severity. These data deserve a dedicated study, especially regarding their spectral contents that would reveal important information about the stiffness of La Jument, hence its health status and remaining lifetime. Also the relative weight on the x and y -peak accelerations that were shown to depart from one extreme wave impact to another (see figure 5) indicates a possible variation in the attack angle of the breaking crest on the lighthouse.

We hope to further investigate the scientific questions raised in this discussion thanks to the extension of the field experiment over several winters and the addition of five pressures sensors, one on the substructure and four on the lighthouse tower, spread over three faces of the octagonal structure.

7. Conclusion

In this paper we have presented observational data from an experiment designed to improve the knowledge of the extreme mechanical loads endured by one of the most iconic lighthouse in France, if not in the world. The dataset, collected during winter 2017-18, contains storm waves and wave-synchronized acceleration data together with tidal current measurements and a high resolution bathymetry. The dataset features several records with significant wave heights above 10m for two of them and giant waves reaching 23.6m high. These observations are completed by numerical wave models results to refine the description of the complex hydrodynamics of La Jument's waters. These models outputs illustrate both the focusing of the wave energy and the chaotic space-time evolution of the wave field in front of La Jument.

In the paper we focused our analysis around an intense and isolated horizontal acceleration burst and showed that it is due to a 19 m-high breaking wave. Our work suggests that this particular wave (wave1) was the only one in the 30 min record analyzed whose crest was high enough to pass above the substructure and reach the lighthouse tower. A series of photographs of wave1 taken for Ushant island supports that the crest hits the concrete belt covering lower part of the tower ([14]). This reveals that the water level during storm events controls the frequency of strong acceleration peaks since the lighthouse substructure acts as a high pass filter for the wave crests. We hope that this ongoing field work will help in quantifying the remaining lifetime of La Jument through a finer description of the incoming waves and of their effect in terms of mechanical loading on the structure.

La Jument is an heritage iconic structure, part of Brittany's culture and known all over the world. Putting aside its role in the navigation safety, it is wise to wonder whether we should spend large amounts of money to maintain a monument that is not accessible to the public. Our scientific experiment demonstrates that this lighthouse, is a unique laboratory to study extreme waves and the loading they induced on marine structures. We believe that its privileged location at the edge of a steep shoal overseeing the open ocean, makes it a favorable site for many other fields of research including wave current interaction, wave breaking or air-sea interface processes. This opportunity could offer a second operational life to La Jument and may justify to maintain this fascinating monument in a decent shape.

Authors' Contributions. JFF drafted the manuscript and analyzed the accelerations and stereo-video times series. PG and AB and RD produced and analyzed the stereo-video surfaces, EL, NF and AV contributed to the accelerations analyses, FL realizes the ray tracing study, MP did the hydrodynamic climatology study, JH and RC were in charge of the X-band investigations, CR was in charge the datawell and AWAC observation study, VR was responsible for the BOSZ modeling, MF and NLD carried out the MBS field survey and analyzed the bathymetric data.

Acknowledgements. We acknowledge the contribution of Peter Sutherland and Mickael Accensi (Ifremer) to the deployment of the stereo-system and Manon Vignes for her help in the relative spatial referencing of the

stereo-video and X band data. We are grateful to from Phares et Balises who allows us to work on La Jument and provides significant support in the preparation and realization of the deployment.

References

- 1 G. B. Airy. Tides and waves. In H. J. Rose et al., editor, *Encyclopedia metropolitana (1817–1845)*. London, 1841.
- 2 Fabrice Ardhuin, Aron Roland, Franck Dumas, Anne-Claire Bennis, Alexei Sentchev, Philippe Forget, Judith Wolf, Françoise Girard, Pedro Osuna, and Michel Benoit. Numerical wave modeling in conditions with strong currents: Dissipation, refraction, and relative wind. *Journal of Physical Oceanography*, 42(12):2101–2120, 2012.
- 3 X Barthelemy, ML Banner, WL Peirson, F Fedele, M Allis, and F Dias. On a unified breaking onset threshold for gravity waves in deep and intermediate depth water. *Journal of Fluid Mechanics*, 841:463–488, 2018.
- 4 J. A. Battjes and J. P. F. M. Janssen. Energy loss and set-up due to breaking of random waves. In *Proceedings of the 16th international conference on coastal engineering*, pages 569–587. ASCE, 1978.
- 5 A. Benetazzo. Measurements of short water waves using stereo matched images sequences. *Coastal Eng.*, 53:1013–1032, 2006.
- 6 Filippo Bergamasco, Andrea Torsello, Mauro Scavo, Francesco Barbariol, and Alvise Benetazzo. Wass: An open-source pipeline for 3d stereo reconstruction of ocean waves. *Computers & Geosciences*, 107:28–36, 2017.
- 7 J.C.N. Borge, K. Reichert, and J. Dittmer. Use of nautical radar as a wave monitoring instrument. *Coastal Eng.*, 37:331–342, 1999.
- 8 Edwige Boudière, Christophe Maisondieu, Fabrice Ardhuin, Mickaël Accensi, Lucia Pineau-Guillou, and Jérémy Lepasqueur. A suitable metocean hindcast database for the design of marine energy converters. *International Journal of Marine Energy*, 3:e40–e52, 2013.
- 9 James Brownjohn, Alison Raby, James Bassitt, Emma Hudson, and Alessandro Antonini. Modal testing of offshore rock lighthouses around the british isles. *Procedia engineering*, 199: 3326–3331, 2017.
- 10 James Mark William Brownjohn, Alison Raby, James Bassitt, Alessandro Antonini, Emma Hudson, and Peter Dobson. Experimental modal analysis of british rock lighthouses. *Marine Structures*, 62:1–22, 2018.
- 11 R. Carrasco, J. Horstmann, and J. Seemann. Significant wave height measured by coherent X-band radar. *IEEE Trans. on Geosci. and Remote Sensing*, 55(9):5355–5365, 2017. doi:10.1109/TGRS.2017.2706067.
- 12 Mayilvahanan Alagan Chella, Alf Tørum, and Dag Myrhaug. An overview of wave impact forces on offshore wind turbine substructures. *Energy Procedia*, 20:217–226, 2012.
- 13 International Electrotechnical Commission. Iec 61400-3. wind turbines—part 3: design requirements for offshore wind turbines. Technical report, 2009.
- 14 Fady N. Denarié, E. Structural behaviour of lighthouses at sea: the case of la jument. *Phil. Trans. Roy. Soc.*
- 15 V. Donato. Laser techniques and applications. In *Proceedings of the Ocean and Coastal Observation Sensors and Systems (OCOSS 2010) conference, Sea Tech Week Congress, 21–25 June 2010. Brest, France.*, pages 43–48. Sea Tech Week, 2010.
- 16 Le Gall B. Erhrhold, A. *Atlas de l'archipel de Molène : géologie, géomorphologie et sédimentologie*. Editions Quae, Versailles, 2017.
- 17 J.-C. Fichou, N. Le Hénaff, and Mével X. *Phares: histoire du balisage et de l'éclairage des côtes de France*. Le chasse marees - ArMen, 1999.
- 18 Y Goda and S Kakizaki. Study on finite amplitude standing waves and their pressure upon a vertical wall. *Rept. Port and Harbour Research Institute*, 5(10):57, 1966.
- 19 S.T. Grilli, I.A. Svendsen, and R. Subramanya. Breaking criterion and characteristics for solitary waves on slopes. *J. of Waterway, Port Coast. Ocean Eng.*, 123(3):102–112, 1997.
- 20 S Hallowell, AT Myers, and SR Arwade. Variability of breaking wave characteristics and impact loads on offshore wind turbines supported by monopiles. *Wind Energy*, 19(2):301–312, 2016.

- 21 W. Huang, R. Carrasco, S. Chengxi, E.W. Gill, and J. Horstmann. Surface current measurements using X-band marine radar with vertical polarization. *IEEE Trans. on Geosci. and Remote Sensing*, 54(5):2988–2996, 2016. doi:10.1109/TGRS.2015.2509781.
- 22 CR Iribarren and C Nogales. Protection des ports, paper presented at xviith international navigation congress, permanent int. *Assoc. of Navig. Congr., Lisbon, Portugal*, 1949.
- 23 Fabien Leckler. *Observation et modélisation du déferlement des vagues*. PhD thesis, Brest, 2013.
- 24 Ning Li, Yoshiki Yamazaki, Volker Roeber, Kwok Fai Cheung, and Gary Chock. Probabilistic mapping of storm-induced coastal inundation for climate change adaptation. *Coastal Engineering*, 133:126–141, 2018.
- 25 Christophe Loraux. Comportement structural des phares en mer, etude historique sur le phare de la jument et propositions d’intervention. Master’s thesis, Maintenance Construction Sécurité (MCS), Ecole Polytechnique Fédérale de Lausanne. mcs.epfl.ch.
- 26 Björn Lund, Brian K Haus, Jochen Horstmann, Hans C Graber, Ruben Carrasco, Nathan JM Laxague, Guillaume Novelli, Cédric M Guigand, and Tamay M Özgökmen. Near-surface current mapping by shipboard marine x-band radar: A validation. *Journal of Atmospheric and Oceanic Technology*, 35(5):1077–1090, 2018.
- 27 A. Miche. Mouvements ondulatoires de la mer en profondeur croissante ou décroissante. forme limite de la houle lors de son déferlement. application aux digues maritimes. Troisième partie. Forme et propriétés des houles limites lors du déferlement. Croissance des vitesses vers la rive. *Annales des Ponts et Chaussées*, Tome 114:369–406, 1944.
- 28 JR Morison, JW Johnson, SA Schaaf, et al. The force exerted by surface waves on piles. *Journal of Petroleum Technology*, 2(05):149–154, 1950.
- 29 Okey Nwogu. Alternative form of Boussinesq equations for nearshore wave propagation. *J. of Waterway, Port Coast. Ocean Eng.*, 119(6):618–637, 1993.
- 30 Le Roux C. Louvart L. Pastol, Y. Litto3d. a seamless digital terrain model. *International Hydrographic Review*, 8.1:38–44, 2007.
- 31 Marc Perlin, Wooyoung Choi, and Zhigang Tian. Breaking waves in deep and intermediate waters. *Annual review of fluid mechanics*, 45:115–145, 2013.
- 32 Owen Phillips, Diafang Gu, and Mark Donelan. Expected structure of extreme waves in a Gaussian sea. part I: Theory and SWADE buoy measurements. *J. Phys. Oceanogr.*, 23:992–1000, 1993.
- 33 Owen Phillips, Diafang Gu, and Edward J. Walsh. Expected structure of extreme waves in a Gaussian sea. part II: SWADE scanning radar altimeter measurements. *J. Phys. Oceanogr.*, 23: 2297–1000, 1993.
- 34 Jeffrey J. Rodriguez and JK Aggarwal. Stochastic analysis of stereo quantization error. *IEEE Transactions on Pattern Analysis and Machine Intelligence*, 12(5):467–470, 1990.
- 35 Volker Roeber and Jeremy D Bricker. Destructive tsunami-like wave generated by surf beat over a coral reef during typhoon haiyan. *Nature Communications*, 6, 2015.
- 36 Volker Roeber and Kwok Fai Cheung. Boussinesq-type model for energetic breaking waves in fringing reef environments. *Coastal Engineering*, 70:1–20, 2012.
- 37 Volker Roeber, Kwok Fai Cheung, and Marcelo H Kobayashi. Shock-capturing boussinesq-type model for nearshore wave processes. *Coastal Engineering*, 57(4):407–423, 2010.
- 38 Etienne S. Scolan, Y.M. Critical jets in a breaking wave. *Actes des 16eme Journees de l’Hydrodynamique*, 27-29 Novembre 2018, Centrale Marseille - IRPHE. URL http://website.ec-nantes.fr/actesjh/images/16JH/Articles/JH2018_papier_09A_Scolan_Etienne.pdf.
- 39 Christian M. Senet, Jörg Seemann, and Friedwart Zeimer. The near-surface current velocity determined from image sequences of the sea surface. *IEEE Trans. on Geosci. and Remote Sensing*, 39(3):492–505, 2001.
- 40 SHOM. Références altimétriques maritimes. côtes du zéro hydrographique et niveaux caractéristiques de la marée, service hydrographique et océanographique de la marine, brest, 2017. URL <https://diffusion.shom.fr/pro/risques/references-verticales/references-altimetriques-maritimes-ram.html>.
- 41 M. Streer, R. Carrasco, and J. Horstmann. Video-based estimation of surface currents using a low-cost quadcopter. *IEEE Geoscience And Remote Sensing Letters*, 14(11):2027–2031, 2017. doi:10.1109/LGRS.2017.2749120.

- 42 Edward B. Thornton and R. T. Guza. Transformation of wave height distribution. *J. Geophys. Res.*, 88(C10):5925–5938, 1983.
- 43 A Varing, JF Filipot, V Roeber, R Duarte, and M Yates-Michelin. A discussion on the wave breaking criterion of shallow water ocean waves. *Actes des 16eme Journees de l'Hydrodynamique, 27-29 Novembre 2018, Centrale Marseille - IRPHE*. URL http://website.ec-nantes.fr/actesjh/images/16JH/Articles/JH2018_papier_09C_Varing_et_al.pdf.
- 44 Norske Veritas. *Recommended Practice DNV-RP-C205: Environmental conditions and environmental loads*. Det Norske Veritas, 2014.
- 45 Th Von Karman. The impact on seaplane floats during landing. 1929.
- 46 J Wienke and H Oumeraci. Breaking wave impact force on a vertical and inclined slender pile—theoretical and large-scale model investigations. *Coastal Engineering*, 52(5):435–462, 2005.
- 47 Jan Wienke, Uwe Sparboom, and Hocine Oumeraci. Breaking wave impact on a slender cylinder. In *Coastal Engineering 2000*, pages 1787–1798. 2001.